

# Competing Ferromagnetic and Charge-Ordered States in Models for Manganites: the Origin of the CMR Effect

Cengiz Şen,<sup>1</sup> Gonzalo Alvarez,<sup>2</sup> and Elbio Dagotto<sup>3,4</sup>

<sup>1</sup>*National High Magnetic Field Laboratory and Department of Physics, Florida State University, Tallahassee, FL 32310*

<sup>2</sup>*Computer Science & Mathematics Division and Center for Nanophase Materials Sciences, Oak Ridge National Laboratory, Oak Ridge, TN 37831*

<sup>3</sup>*Materials Science and Technology Division, Oak Ridge National Laboratory, Oak Ridge, TN 32831*

<sup>4</sup>*Department of Physics and Astronomy, The University of Tennessee, Knoxville, TN 37996*

(Dated: March 23, 2022)

The one-orbital model for manganites with cooperative phonons and superexchange coupling  $J_{AF}$  has been investigated via large-scale Monte Carlo (MC) simulations. Results for two-orbitals are also briefly discussed. Focusing on electronic density  $n=0.75$ , a regime of competition between ferromagnetic (FM) metallic and charge-ordered (CO) insulating states was identified. In the vicinity of the associated bicritical point, colossal magnetoresistance (CMR) effects were observed. The CMR is associated with the development of short-distance correlations among polarons, above the spin ordering temperatures, resembling the charge arrangement of the low-temperature CO state.

PACS numbers: 75.47.Lx, 75.30.Mb, 75.30.Kz

*Introduction:* The colossal magnetoresistance of the manganites is an example of the complex behavior and nonlinearities that can emerge in materials where several degrees of freedom are simultaneously active [1, 2]. Understanding theoretically the CMR effect is important not only for its intrinsic value in the Mn oxide context, but also to provide a paradigm for rationalizing a plethora of related complex phenomena unveiled in several other transition metal oxides in recent years [3]. The current scenarios to understand the CMR behavior rely on the existence of competing states and the emergence of nanometer-scale electronic structures [2]. Using simple models of phase competition (valid at large length scales) and resistor-network approximations, CMR behavior was observed [4]. However, for a deeper understanding, it is imperative to unveil the CMR effect in more fundamental microscopic models, using fully unbiased many-body techniques to handle the strong interactions. Along this line, considerable progress was recently made with the report of large magnetoresistance effects in Mn-oxides models in the case where the double-exchange (DE) induced FM metal competes with a FM insulator made out of randomly localized polarons [5, 6, 7]. However, a complete rationalization of CMR physics needs a CO antiferromagnetic (AF) state as the true competitor of the FM metal, since it is under these circumstances that the magnetoresistance effect is truly colossal [1, 2]. For this goal, it is crucial to incorporate the  $t_{2g}$  AF superexchange  $J_{AF}$ , known to be fundamental to reproduce the CO-AF states observed in real manganite phase diagrams [2].

The main purpose of this manuscript is to present large-scale computational studies of models for manganites, incorporating now explicitly the  $J_{AF}$  interaction. The main result is that a CMR effect, with CMR ratios as large as 10,000%, is unveiled using realistic models and electronic densities, and unbiased methods. The  $J_{AF}$

coupling is shown to be crucial for the magnitude of the effect. A simple picture for the origin of the CMR effect is discussed, that relies on nanometer-scale short-range order above the Curie temperature  $T_C$ , in qualitative agreement with previously proposed mixed-phase scenarios. The comprehensive investigation reported here was possible by using hundreds of nodes of the Cray XT3 supercomputer operated by the National Center for Computational Studies, at Oak Ridge National Laboratory (ORNL). The same effort on conventional PC clusters would have demanded several years for completion.

*Models and Techniques:* The models and methodology used in this effort have been extensively discussed before [2, 7]. Then, only a brief description is here included. The one-orbital Hamiltonian is given by  $H=H_{1b}+H_{AF}$ , where  $H_{1b}$  contains the standard fermionic nearest-neighbor (NN) hopping term at infinite Hund's coupling, plus the interaction with the oxygen phonons which are assumed classical. The full  $H_{1b}$  term, including on-site disorder, is explicitly defined in Eq.(2) of Ref. 7. The two-orbital model, also used here, is identical to Eq.(4) of Ref. 7. The electron-phonon coupling is denoted by  $\lambda$ , the strength of the on-site quenched disorder is  $\Delta$ , the chemical potential  $\mu$  regulates the density  $n$ , and the hopping  $t=1$  is the energy unit [8]. In this study, the second term  $H_{AF}=J_{AF}\sum_{\langle ij\rangle}\vec{S}_i\cdot\vec{S}_j$  plays a key role. This interaction represents the NN superexchange, with coupling  $J_{AF}$ , between the (assumed classical)  $t_{2g}$  spins  $\vec{S}_i$ . The study of this model involves the standard exact diagonalization of the fermionic sector for a given classical phononic and  $t_{2g}$  spins configuration, updated via a MC procedure [2]. The charge-charge correlations were evaluated using  $C(j)=(1/N)\sum_i(\langle n_i n_{i+j} \rangle - \langle n \rangle^2)$  with  $n_i$  the electronic density at site  $i$ , and  $N$  the total number of sites. The resistivity  $\rho$  has been calculated by taking the inverse of the mean conductivity  $\sigma$ , where the

latter is related to the conductance  $G$  by  $G=\sigma L^{d-2}$ ,  $d$  being the dimension, and  $L$  the linear size of the lattice. The conductance  $G$  was obtained using the Kubo formula [9]. For further details, the reader should consult Sec. II of Ref. 7. Finally, note that finite clusters do not lead to true singularities, such as a critical temperatures. However, decades of investigations in a wide variety of contexts have shown that finite systems can accurately capture the rapid growth of correlation lengths in narrow temperature ranges expected from criticality. These temperatures can be safely associated with true critical temperatures, and this is the convention followed here and in many previous studies [2, 4, 5, 6, 7].

*Clean-Limit Phase Diagram:* The key novelty of this investigation is the existence of an insulating CO/AF state competing with the FM metal to generate the CMR. In Fig. 1, the clean-limit  $\Delta=0$  one  $e_g$ -orbital model phase diagram is presented, at an experimentally realistic density  $n=0.75$  and intermediate  $\lambda=1.2$ . At  $J_{AF}=0$ , the ground state is a DE generated standard FM metal, with charge uniformly distributed. With increasing  $J_{AF}$ , a first-order transition occurs to a CO/AF state schematically shown in Fig. 1 [10]. The holes are arranged regularly, separated by distances 2 and  $\sqrt{5}$ . This state is degenerate with a state rotated in  $90^\circ$ . The spins are also indicated. This type of states are the analog of the more realistic CO/AF states that exist in two-orbital Mn-oxide models, such as the CE state [2].

*Clean-limit CMR:* The most important result of these investigations is shown in Fig. 2, where the  $\rho$  vs. temperature  $T$  curves are shown. Consider Fig. 2(a): here  $\rho$  vs.  $T$  presents the expected insulating behavior at large  $J_{AF}$ , and the canonical bad-metal DE form at small  $J_{AF}$  (or reducing  $\lambda$ ). The remarkable result appears in between, mainly in the narrow  $J_{AF}$  interval approximately between 0.02 and 0.0325. In this regime,  $\rho$  vs.  $T$  presents a canonical CMR shape, with insulating behavior at large  $T$ , transforming into a broad high peak upon cooling (logarithm scale used), followed by metallic behavior at low  $T$ . The  $T_C$  is approximately located at the resistivity peak. This is in agreement with the experimental phenomenology of CMR manganites, and with the theoretical scenarios [2, 4] based on a CMR emerging from phase competition between a FM metal and a CO-AF insulator. The result is particularly remarkable considering the relatively small clusters used in our studies: the origin of the CMR effect unveiled here must lie in phenomena occurring at the nanometer scale, as recently remarked [11]. The only “price” to pay is the tuning of couplings: the CMR shape is obtained in narrow intervals  $\Delta\lambda\sim 0.1$  (inset Fig. 2(a)) and  $\Delta J_{AF}\sim 0.02$ . However, this delicate tuning is removed by adding quenched disorder, as shown before [4, 6, 7], and also below in the present effort.

In Figs. 2(b,c), the effects of magnetic fields  $H$  are shown. In agreement with experiments, the peak in  $\rho$  is strongly suppressed by magnetic fields that are small

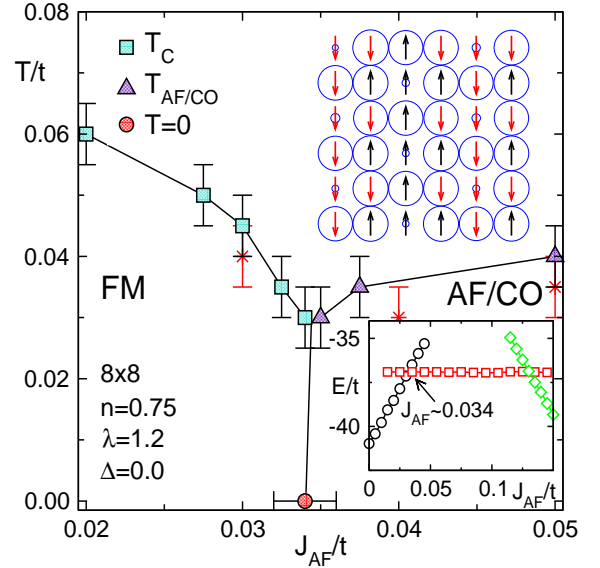


FIG. 1: (Color online) Clean limit MC phase diagram using  $8\times 8$  and  $12\times 12$  lattices, at  $n=0.75$  and  $\lambda=1.2$ . The AF/CO state is schematically shown, with the radius of the circles proportional to the electronic density, and arrows representing the  $t_{2g}$  spins. Charge is uniform in the competing FM state. At each temperature,  $1\times 10^5$  thermalization and  $5\times 10^4$  measurement MC steps were carried out for the  $8\times 8$  clusters (and  $\sim 7500$  and  $5000$ , respectively, for the  $12\times 12$  cluster points indicated by red stars). Random starting spin configurations were used in all simulations, but the results have also been checked for convergence using ordered starting configurations.  $T_C$  is defined as the temperature where the spin-spin correlations at the maximum cluster distance nearly vanish. Similarly,  $T_{AF/CO}$  is the temperature where both AF and FM correlations vanish at the maximum allowed distances. At  $T_{AF/CO}$ , the charge structure factor  $n(\mathbf{q})$  at  $\mathbf{q} = \mathbf{q}_{CO}$  also vanishes. *Inset:* energy vs.  $J_{AF}$  at very low  $T\sim 0$ , with the FM (CO/AF) phase in black (red). Green dots indicate a G-ordered AF regime. Here, the spins were frozen to their expected states and the phonons were MC relaxed.

in the natural units  $t=1$ . The concomitant CMR ratios  $[(\rho(0)-\rho(H))/\rho(H)]\times 100\%$  are as large as 10,000%. The comparison between  $8\times 8$  and  $12\times 12$  clusters also show that size effects are mild in these investigations.

*Influence of Quenched Disorder, Dimensionality, and Number of Orbitals:* Fig. 3(a) shows typical  $\rho$  vs.  $T$  curves in the presence of on-site-energy quenched disorder. As discussed before [6, 7], the disorder enhances the tendency toward having  $\rho$  vs.  $T$  curves with the canonical CMR shape, and the fine tuning problem is avoided. This is important to rationalize the universality of the CMR effect, present in so many Mn oxides that they cannot all be finely tuned to the same couplings.

To complete our investigations, the effects of dimensionality and orbital number were also addressed. In Fig. 3(b) results are shown using a  $4\times 4\times 4$  cluster, as a representative of a 3D lattice, in the clean limit. The  $\rho$  vs.  $T$  curves are very similar to those found in 2D sys-

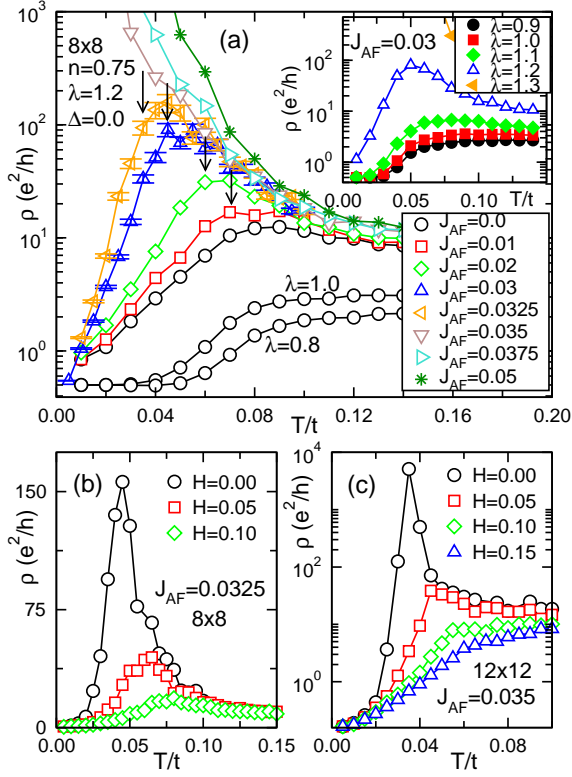


FIG. 2: (Color online) Resistivity  $\rho$  vs  $T$  curves for various parameters: (a) Fixing  $\lambda=1.2$  and varying  $J_{AF}$ . Arrows indicate  $T_C$ 's. Results at  $\lambda=0.8$  and  $\lambda=1.0$ , with  $J_{AF}=0.0$ , are also shown. *Inset*: results fixing  $J_{AF}=0.03$  and varying  $\lambda$ . (b) Effect of magnetic fields (indicated, in  $t$  units) on  $\rho$  using  $J_{AF}=0.0325$ , on an  $8 \times 8$  lattice. (c) Same as (b) but for  $J_{AF}=0.035$ , on a  $12 \times 12$  lattice. In (a) and (b), MC steps and the starting configurations are the same as in Fig. 1. In (c), 7500 thermalization and 5000 measurement steps were used. Typical error bars are indicated in (a).

tems. In Fig. 3(c), results using a two-orbital model are presented, with similar conclusions. Figure 3(c) and others not shown, suggest that the results are qualitatively the same for the one- and two-orbital models [12].

*Understanding the CMR Effect:* To understand the CMR effect found here, it is important to analyze short-distance charge correlations above the ordering temperatures. In particular, the correlations at distance  $\sqrt{5}$ , denoted  $C(\sqrt{5})$ , are important since they are robust in wide ranges of temperatures and couplings, they are ubiquitous in most MC snapshots, and of course they are also characteristic of the CO/AF state in Fig. 1. A clear relation between  $C(\sqrt{5})$  and  $\rho$  is shown in Fig. 4(a), where they are plotted together for a representative  $J_{AF}$ . In the regime below a new characteristic temperature  $T^* \sim 0.15$ , both quantities nicely track each other, showing that the increase of short-distance charge correlations causes the increase in  $\rho$  upon cooling. This figure is conceptually similar to Fig. 4 of Ref. 13, where  $\rho$  for  $\text{La}_{0.7}\text{Ca}_{0.3}\text{MnO}_3$  was shown together with the neu-

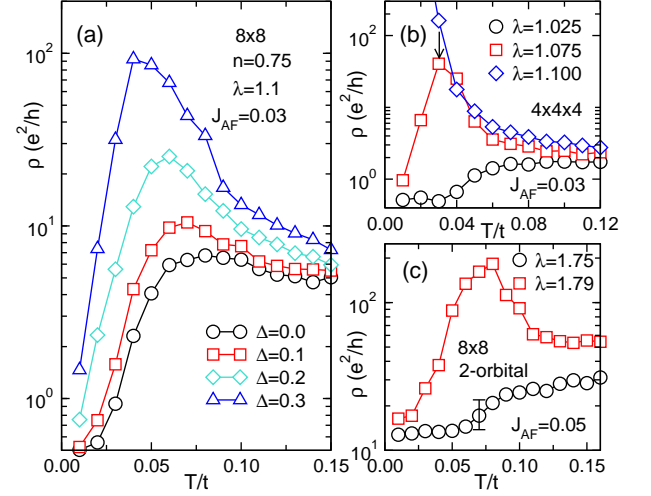


FIG. 3: (Color online) (a)  $\rho$  vs.  $T$  in the presence of quenched disorder  $\Delta$ . Up to ten different disorder realizations were used in calculations with quenched disorder. Only small changes between configurations were observed. MC steps and starting configurations are as in Fig. 1. (b)  $\rho$  vs.  $T$  using a  $4 \times 4 \times 4$  lattice, parametrized with  $\lambda$ , at  $J_{AF}=0.03$ . (c) Two orbitals  $\rho$  vs.  $T$  results using an  $8 \times 8$  lattice for  $J_{AF}=0.05$ . In (b) and (c), 4000 thermalization and 4000 measurement MC steps were used,  $n=0.75$ , and the clean limit  $\Delta=0$  was studied.

tron scattering  $(1/4, 1/4, 0)$  polaron peak that describes short-distance polaron correlations. Such a “correlated polaron” signal is the analogous of short-range CO in our one-band model, a precursor of the CO state stabilized at low  $T$  close in parameter space. Figure 4(a) shows that the short-distance charge order is reduced at low  $T$  but it does not disappear: in this regime the FM order of the spins, together with some reduction in charge correlations, causes the dramatic resistance drop.

The scale  $T^*$  where short-range correlations start to build up was already predicted based on phenomenological investigations [4], it was also found experimentally [14], but had not been reported before using basic models for manganites. The resistivity becomes nearly flat above  $T^*$ . In our investigations, a pseudogap (PG) in the density-of-states  $N(\omega)$  was also observed [15], and its inverse at  $\mu$  is shown in Fig. 4(a). The PG disappears at a higher temperature  $T^{pl}$ , probably related to polaron formation. The resistivity is not affected by  $T^{pl}$ , but upon further cooling to  $T^*$  those polarons become correlated and  $\rho$  dramatically increases [16].

Finally, while averaged quantities are certainly crucial for quantitative studies, the “by eye” examination of MC snapshots is also illustrative. In Fig. 4(b), a typical snapshot in the CMR regime is shown. Pairs of holes located at the distances  $\sqrt{5}$  and 2 are highlighted. Clearly, MC equilibrated configurations do *not* have randomly distributed holes (i.e., it is not a gas of heavy polarons), but special distances are preferred over others: the polarons are correlated. Those distances are the same that

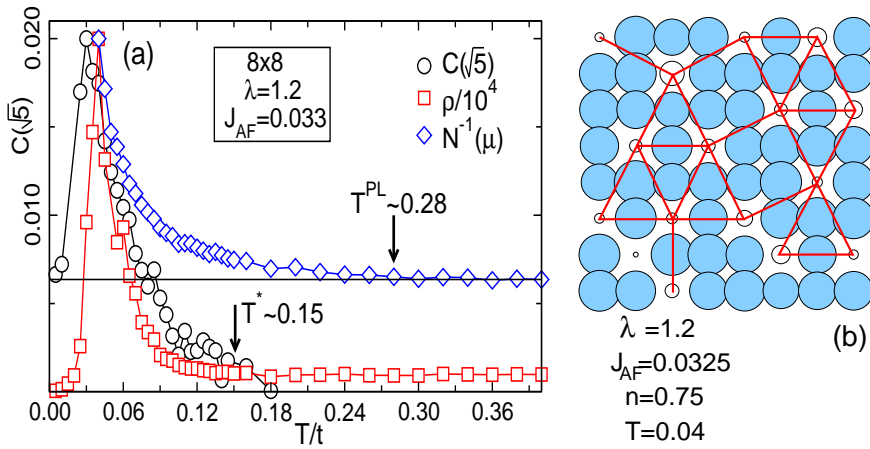


FIG. 4: (Color online) (a) MC averaged  $C(\sqrt{5})$  vs.  $T$ , showing a qualitative similarity with the rescaled resistivity (also shown). This agreement occurs below the  $T^*$  indicated. At higher  $T$ ,  $\rho$  is flat and  $C(\sqrt{5})$  nearly vanishes. Also shown is the inverse of  $N(\omega = \mu)$ , to indicate the PG formation at  $T^{pl}$ . (b) Typical MC snapshot with the radius of the circles proportional to the local charge density. Also shown are the hole-hole distances  $\sqrt{5}$  and  $2$  of relevance (see text).

characterize the low- $T$  CO state (Fig. 1). Also, in the MC snapshots the  $t_{2g}$  spins at the hole locations and their four neighbors were found to be polarized similarly to that shown in Fig. 1. Thus, puddles of the CO-AF state appear in the MC snapshots, and their existence is correlated with the shape of the  $\rho$  vs.  $T$  curves.

**Conclusions:** The results reported here show that realistic models for manganites – with the DE, electron-phonon, and  $J_{AF}$  interactions – can explain the CMR effect and its magnitude. The coupling  $J_{AF}$  is crucial, since it is needed to stabilize the CO-AF state that competes with the FM metal. The origin of the CMR is the formation of nano-scale regions above  $T_C$ , with the same charge and spin pattern as the low- $T$  insulating CO-AF state. To obtain CMR effects, clusters of just a few lattice spacings in size appear sufficient [11]. Our results show that the CMR effect is much larger when the insulating competing state has charge ordering tendencies, as opposed to having merely randomly localized polarons. The latter state has been recently identified using STM techniques, in a bilayered  $x=0.3$  manganite with mild in-plane magnetoresistance [17]. If the same STM experiment is repeated at  $x=0.4$ , where the CMR is much stronger, it is predicted that *aggregates* of polarons resembling a CO state should be observed above  $T_C$ .

**Acknowledgment:** We acknowledge discussions with D. Argyriou, S. Kumar, J. W. Lynn, P. Majumdar, and R. Mathieu, and support via the NSF grant DMR-0443144 and the LDRD program at ORNL. Most of the computational work was performed on the Cray XT3 of the Center for Computational Science at ORNL, managed by UT-Battelle, LLC, for the U.S. Department of Energy under Contract DE-AC05-000R22725. This research used the SPF computer program and software toolkit developed at ORNL (<http://mri-fre.ornl.gov/spf>).

- Phys. **73**, 583 (2001); J. De Teresa *et al.*, Nature **386**, 256 (1997); M. Uehara *et al.*, Nature **399**, 560 (1999).
- [2] E. Dagotto *et al.*, Phys. Rep. **344**, 1 (2001); A. Moreo *et al.*, Science **283**, 2034 (1999).
- [3] E. Dagotto, Science **309**, 258 (2005).
- [4] J. Burgý *et al.*, Phys. Rev. Lett. **87**, 277202 (2001); *ibid.*, Phys. Rev. Lett. **92**, 097202 (2004).
- [5] J. A. Vergés *et al.*, Phys. Rev. Lett. **88**, 136401 (2002).
- [6] S. Kumar and P. Majumdar, Phys. Rev. Lett. **96**, 016602 (2006); *ibid.*, Phys. Rev. Lett. **94**, 136601 (2005); cond-mat/0503746.
- [7] C. Sen *et al.*, Phys. Rev. B **73**, 224441 (2006).
- [8] The effects of the Hubbard repulsion are mild at large Hund coupling, since it prevents double occupancy [2], and repulsions can be absorbed in redefined couplings (T. Hotta *et al.*, Phys. Rev. B **62**, 9432 (2000)).
- [9] J. A. Vergés, Comput. Phys. Commun. **118**, 71 (1999).
- [10] “Bicritical” phase diagrams are theoretically expected and they have been observed experimentally: Y. Tomioka and Y. Tokura, Phys. Rev. B **70**, 014432 (2004).
- [11] R. Mathieu *et al.*, Phys. Rev. Lett. **93**, 227202 (2004). See also the *CE glass* concept introduced in H. Aliaga *et al.*, Phys. Rev. B **68**, 104405 (2003) and Y. Motome *et al.*, Phys. Rev. Lett. **91**, 167204 (2003).
- [12] However, note that the study of an individual parameter set for the two-orbital model costs 16 times more than for one orbital, since the computational effort scales as the number of degrees of freedom to the 4th power.
- [13] C. P. Adams *et al.*, Phys. Rev. Lett. **85**, 3954 (2000).
- [14] D. N. Argyriou *et al.*, Phys. Rev. Lett. **89**, 036401 (2002). J. W. Lynn *et al.*, preprint; D. Dessau *et al.*, preprint.
- [15] D. Dessau *et al.*, Phys. Rev. Lett. **81**, 192 (1998); A. Moreo *et al.*, Phys. Rev. Lett. **83**, 2773 (1999).
- [16] CMR needs correlated polarons: a simple small-polaron picture for the CMR state has been recently ruled out (E. Bozin *et al.*, cond-mat/0609485).
- [17] H. M. Ronnow *et al.*, Nature **440**, 1025 (2006).

[1] Y. Tokura, *Colossal Magnetoresistance Oxides* (Gordon and Breach, 2000); M. Salamon and M. Jaime, Rev. Mod.